

Cluster size dependence of high-order harmonic generation

Y. Tao¹, S. J. Goh¹, H. M. J. Bastiaens¹, P. J. M. van der Slot¹, S. G. Biedron², S. V. Milton² and K. -J. Boller¹

¹ Laser Physics and Nonlinear Optics, Department of Science and Technology, MESA+ Institute for Nanotechnology, University of Twente, Enschede, The Netherlands

² Department of Electrical and Computer Engineering, Colorado State University, Fort Collins, Colorado, USA

E-mail: y.tao-1@utwente.nl

25th Nov 2016

Abstract. We investigate high-order harmonic generation (HHG) from noble gas clusters in a supersonic gas jet. To identify the contribution of harmonic generation from clusters versus that from gas monomers, we measure the high-order harmonic output over a broad range of the total atomic number density in the jet (from $3 \times 10^{16} \text{ cm}^{-3}$ to $3 \times 10^{18} \text{ cm}^{-3}$) at two different reservoir temperatures (303 K and 363 K). For the first time in the evaluation of the harmonic yield in such measurements, the variation of the liquid mass fraction, g , versus pressure and temperature is taken into consideration, which we determine, reliably and consistently, to be below 20% within our range of experimental parameters. Based on measurements with a thin jet where significant variations in reabsorption and the phase matching conditions can be neglected, we conclude that atoms in the form of small clusters (average cluster size < 1000 atoms) provide the same higher-order nonlinear response as single-atoms. This implies that HHG in small clusters is based on electrons that return to their parent ions and not to neighbouring ions in the cluster. This conclusion is consistent with the measured harmonic spectra showing no obvious changes of the cut-off wavelength. Our results are in clear contrast to previous work concluding that the single-atom response in small clusters increases with the cluster size, thereby promising a higher output than with monomers. Cluster may still increase the yield of high-order harmonic generation, however, not via the single-atom response but possibly via quasi-phase matching, as the higher mass of clusters allows for a higher density contrast in spatially structuring the nonlinear medium.

Keywords: cluster, liquid mass fraction, nonlinearity

Submitted to: *New J. Phys.*

1. Introduction

Table-top sources based on high-order harmonic generation (HHG) provide coherent extreme ultraviolet (XUV) radiation on the femtosecond or even attosecond timescale [1]. Such radiation is of great interest for various applications such as probing the ultrafast dynamics of atomic, molecular and solid systems [2], lensless diffractive imaging of objects at the nanoscale [3], as well as seeding free-electron lasers [4]. Typically, noble gas atoms serve as the medium for HHG. On the single-atom level, the mechanism of such a process can be intuitively understood within a simple three-step model [5, 6]: Initially, an electron escapes from its bound state in a strong drive laser field through tunnel ionization. Secondly, the electron is driven away and then accelerated back towards its parent ion. Finally, the electron recombines with its parent ion. However, in spite of progress with phase matching, the macroscopic output remains low [7, 8, 9]. Recently, HHG from crystalline solid materials [10, 11, 12] has been discovered and has shown a potential for higher conversion efficiency owing to the high density in solids. In addition, solids can be structured periodically on a micrometer scale which might further enable quasi-phase matching [13]. However, the generation mechanism of HHG in solids differs fundamentally from that in gas atoms. Unlike the atomic three-step model, knowledge of the complex electron dynamics inside the periodic structure of solids, responsible for the generation of harmonics, is missing. Moreover, in order to prevent permanent damage of the crystal, the drive laser intensities in those experiments are at least one order of magnitude lower than those conventionally applied in the gas medium, which results in a rather low cut-off energy [12].

Nanometer-sized clusters, formed via the van-der-Waals aggregation of gas atoms or molecules, provide an attractive alternative for HHG [14, 15, 16, 17, 18, 19] since they combine the low average density of gas and the local high density of solids and liquids. This unique property should allow one to investigate the mechanism of HHG across the full range of relative densities from individual atoms up to solid materials. Furthermore, clusters have been shown as suitable to form spatially tailored density distributions that can be used for direct acceleration of particles [20], an avenue that appears promising also for achieving quasi-phase matching in HHG.

However, the exact mechanism of HHG in clusters is not clear, e.g., it is not known to what extent the simple three-step model remains applicable for describing HHG in clusters. In particular, the recollision mechanism in the three-step model for clusters is not clarified yet. Several reports have attempted to improve the understanding of the mechanism of HHG based on their more detailed experimental observations. Donnelly et al. [14], Vozzi et al. [16] and Aladi et al. [21] observed an extended cut-off energy and enhanced conversion efficiency in clusters. The results suggest that the electron is initially tunnel ionized from one atom and later recollides with another neighbouring atom (atom-to-neighbour) instead of recombining with its parent atom (atom-to-itself). Such a mechanism would result in the generation of Bremsstrahlung (incoherent, broadband emission). Meanwhile, both Ruf et al. [17] and Park et al. [18]

proposed another recollisional mechanism (cluster-to-itself). In that scenario, the harmonic radiation is assumed to be generated from a partially delocalized wave function spreading over the whole cluster. This is supported by measuring the ellipticity as well as the group delay of the high-order harmonics from clusters. An alternative recollision mechanism occurring in overdense plasmas [22] or solids [10] may also exist. Besides, resonant heating [23] mechanism can also occur during the tunnel ionization process.

In addition to these microscopic atomic-scale phenomena, HHG is a coherent emission process, such that the yield is also strongly affected by the macroscopic aspect, specifically phase matching, while further modifications can be caused by reabsorption of generated harmonics along the interaction length. Correspondingly, it is not easy to disentangle the single particle (gas monomer or cluster) contribution from an experimental point of view. When attempting a measurement of the intrinsic (microscopic) nonlinear response of clusters versus their size, several considerations are of importance in an experiment. Generally, clusters are produced in a supersonic jet expansion of inert gas atoms. Both the average cluster size and density can be well controlled by the stagnation pressure and reservoir temperature [24, 25]. However, when tuning these two experimental parameters, it is required to carefully keep the measured data, e.g., the generated harmonic order, away from ranges where strong phase mismatch and absorption limit or strongly influence the output signals. This is to ensure that the signals are large enough to be measurable by the detection system [18]. Moreover, except for the average cluster size and density, there is another important parameter, the liquid mass fraction, g , which characterizes the formation of clusters. This parameter is defined as the ratio of the number of atoms in the form of clusters to the total number of atoms in the jet. For most of the experiments mentioned above [15, 16, 18, 19], the researchers interpret their results by choosing $g=1$ without further justification, namely, they assume that a pure cluster jet is generated and thereby the measured high-order harmonic (HH) signals are *entirely* to be attributed to clusters. However, both our recent modelling of cluster formation [26] and other measurements [27, 28] strongly indicate that g is not unity but dependent on both the stagnation pressure and reservoir temperature. For instance, the value of g for argon clusters lies only at about 20% at room temperature over a broad range of stagnation pressures. Even at very low reservoir temperatures (~ 173 K, via cooling by pre-cooled nitrogen gas [28]), g only rises up to $\sim 40\%$. As a result, the assumption of $g = 1$ misleads the interpretation of the measurements. For a valid determination of the nonlinearity of clusters, one has to take into account the contribution to the HH yield from both clusters as well as gas monomers when interpreting experimental data.

In this work, we present a detailed experimental study on HHG from a supersonic argon jet. To identify a possible dependence of HHG on the average cluster size, we change the stagnation pressure over a broad range to maximize the variation in cluster size. For disentangling the contribution to HHG from clusters and gas monomers, we perform experiments at two different reservoir temperatures in order to vary the liquid mass fraction, g , for the same range of cluster sizes. We determine the dependence of

the liquid mass fraction, g , on both stagnation pressure and reservoir temperature with a high degree of reliability using our one-dimensional model [26]. We find that about a maximum of 20% of the gas atoms are converted into clusters under our experimental conditions. Combining this value of g with the density dependent measurement of the HH spectra, we show that small argon clusters below 1000 atoms per cluster have the same single-atom response as gas monomers. For clusters having larger cluster sizes, the single-atom response becomes smaller. This result is in contrast to earlier work [18] that concludes an increased nonlinearity of atoms in clusters when $\langle N \rangle$ is smaller than 700 atoms per cluster. Moreover, we observe no changes in the cut-off energy when the average cluster size increases. This confirms other reports [18] suggesting that the collision mechanism described in the three-step model for HHG in gas atoms may still be applicable for HHG in clusters. This means that the tunnelled electron recombines only with its parent ion.

2. Experimental setup

The experimental setup used for HHG in clusters is depicted in Fig. 1. Argon clusters are generated from a supersonic slit nozzle (rectangular cross section of exit: 1.0×5.0 mm², expansion half-angle: 14°) mounted on top of an electro-magnet driven pulsed gas valve (Parker, 9 series) inside a vacuum chamber. The stagnation pressure applied to the valve can be varied between 0 and 70 bar, with an accuracy of 0.2 bar at low pressures (0 to 5 bar), and with an accuracy of 0.5 bar in the higher pressure regime (5 to 70 bar). With a resistive heater, the temperature of the nozzle can be adjusted between room temperature and 105°C with an accuracy of about 0.5°C . The average cluster size and density, as well as the total atomic number density generated with the supersonic nozzle were measured as a function of stagnation pressure at different temperatures as presented in our previous published paper [26]. To exclude the influence of changing phase matching conditions in the build-up of the harmonic field, the slit nozzle is oriented perpendicular to the drive laser beam, such that the laser beam propagates through the short dimension (width) of the jet ensuring that the interaction length is shorter than the coherence length. For driving HHG, we employ a femtosecond Ti:Sapphire laser system operating at a center wavelength of 795 nm at 1 kHz repetition rate (Legend Elite Duo HP USP, Coherent Inc.). The laser generates linearly polarized output pulses with a maximum pulse energy of 6.5 mJ and a pulse duration of about 40 fs [29]. To avoid any major self-phase modulation and plasma defocusing along the propagation direction, the pulse energy used in our experiment is limited to a fixed value of 3.0 mJ via a variable attenuator comprising a rotatable half-wave plate followed by a thin film polarizing beam splitter (PBS). The laser pulse is loosely focused about 1 mm above the nozzle using a lens of 1200 mm focal length, resulting in a peak intensity of about 1.5×10^{14} W/cm² at focus and an effective interaction length [26] of about 650 μm . The relatively low peak intensity and short pulse duration ensures that the harmonic emission involves only clusters that are not already affected by ionization induced explosion and

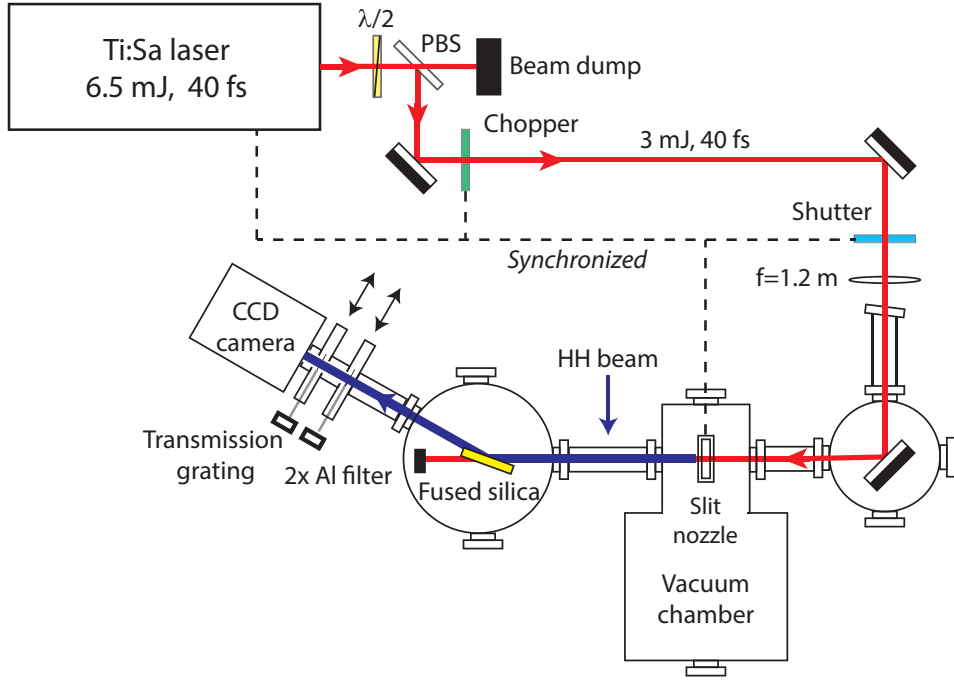


Figure 1: Schematic of the experimental setup for HHG in an argon supersonic jet.

disintegration, since the time scale for these processes (\sim hundreds of femtoseconds) is much longer than the drive laser pulse duration (~ 40 fs) [18]. The generated HH beam co-propagates with the drive laser beam, from which it is primarily separated by an uncoated fused silica plate placed at an incident angle of 75 degree. This incident angle is close to the Brewster angle for the drive laser beam (at center wavelength), such that most of the drive laser beam is transmitted and diverted to an absorbing beam dump. Any residual drive laser radiation that is reflected from the fused silica plate is fully blocked by a set of two 200-nm thick aluminium (Al) filters placed in series. These filters act as a band pass filter for the harmonic radiation, transmitting more than 40% in the wavelength range of 17 to 80 nm [30]. The transmitted HH beam is detected by an XUV CCD camera (Princeton Instruments, PIXIS-XO 2048B) placed behind the filters. For the measurement of the spectral distribution of the HH output, an in-house fabricated transmission grating (3,000 lines/mm) [30] illuminated through a $300 \mu\text{m}$ slit is shifted into the beam path. To minimize absorption of HH radiation in the beam path towards the detection system, the pulsed gas valve is operated at a low repetition rate of 1 Hz, as to keep the background pressure below 10^{-3} mbar during operation. A mechanical chopper system (MC20008B-EC, Thorlabs Inc) is inserted into the beam path, which reduces the repetition rate of the drive laser from 1 kHz to 71 Hz, in order to prevent any damage to the fused silica plate and the Al filters due to high average power. For allowing the single-shot detection of the HH beam profile, an additional mechanical shutter (SH05, Thorlabs Inc) could be inserted into the beam path, reducing the repetition rate of the laser further to 1 Hz.

3. Result and Discussion

As was emphasized above, it is essential for correct data interpretation that the influence of the liquid mass fraction, g , on the HH yield is clarified, because only this enables us to resolve the relative contribution from clusters and gas monomers. Here, we first determine the dependence of the liquid mass fraction, g , on the two main experimental parameters, which are the stagnation pressure, p_0 , and the reservoir temperature, T_0 . An understanding of this dependence is required for the analysis of the scaling of the measured HH intensity with the stagnation pressure (which determines the atomic number density) as shown below. Next, we discuss the HH spectra and the cut-off wavelength measured for two specific temperatures, at three different stagnation pressures. From these spectra, we extract and compare the spectrally integrated HH signal measured at two different temperatures. Importantly, we show that, in the low-pressure regime, the measured HH signal is not dominated by absorption and phase mismatch which is another essential ingredient for appropriate interpretation of the data. Finally, using a simple model describing the dependence of the harmonic yield on the total atomic number density as well as the average cluster size, we analyze the relative contribution of clusters and gas atoms with regard to the liquid mass fraction. From this, we obtain the single-atom response for clusters with different sizes.

Fig. 2 shows the liquid mass fraction, g , across a broad range of stagnation pressures, p_0 , (from 300 mbar to 35 bar), and the two reservoir temperatures, ($T_1 = 303$ K and $T_2 = 363$ K) used in the HHG experiments. To determine g , we have used the relation that we derived previously by combining interferometry and Rayleigh scattering data with a theoretical description of cluster formation [26]. To allow a direct comparison of the liquid mass fraction at different temperatures, the stagnation pressure is converted into the total atomic number density, $n_a \propto p_0/T_0$, calibrated by an interferometric measurement [26]. It can be seen that the liquid mass fraction is far off unity in that it grows from extremely small values (near zero) to a maximum of about 19%. The inset shows an enlarged view of the growth of g in the low-density region up to $n_a = 5 \times 10^{17} \text{ cm}^{-3}$. From Fig. 2, it can be clearly seen that, at $T_1 = 303$ K (black squares), the liquid mass fraction is very small (≤ 0.01) for densities up to $n_a = 10^{17} \text{ cm}^{-3}$, and increases rapidly up to 10% at a density of about $n_a = 1.8 \times 10^{17} \text{ cm}^{-3}$. Above this density, g grows more weakly, reaching its maximum value of about 19% for a density near $n_a = 2.5 \times 10^{18} \text{ cm}^{-3}$. The growth trend of the liquid mass fraction at increased temperature, $T_2 = 363$ K (red circles), is very similar, although setting in at a higher density of about $n_a = 2 \times 10^{17} \text{ cm}^{-3}$. In this case, g reaches a value of 16% for a density around $n_a = 2.5 \times 10^{18} \text{ cm}^{-3}$. Within the entire range of the densities and temperatures accessible in our experiment, we find that the liquid mass fraction remains lower than 19%. We note that these rather low values for g correspond well with the experimental results reported by others [28, 31]. Our modelling results show that even at cryogenic temperatures (at 170 K, which can be achieved using pre-cooled nitrogen gas) and high stagnation pressures (50 bar) the maximum liquid

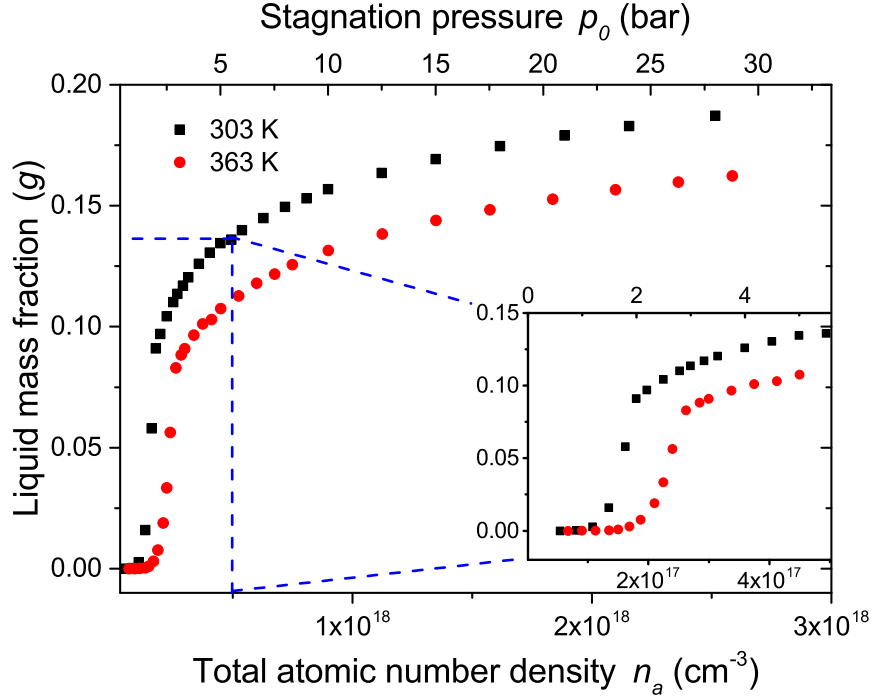


Figure 2: Liquid mass fraction, g , in the supersonic argon jet as a function of the total atomic number density, n_a , for two different reservoir temperatures ($T_1 = 303$ K and $T_2 = 363$ K), as obtained from Ref [26].

mass fraction still does not rise above 40%. From this we conclude that all the previous experimental investigations aiming to unravel the size dependent cluster contribution to the HH yield from the supersonic gas jet have provided questionable conclusions as it is not justified to neglect the major presence of atoms as monomers [16, 18].

To study more quantitatively the influence of the liquid mass fraction on the HH yield, we raise the temperature of the nozzle to decrease g , while keeping the total atomic number density in the jet unchanged. This is accomplished by increasing the stagnation pressure such that the ratio p_0/T_0 remains constant. In Fig. 3, we present a series of six typical HH spectra measured at two specific temperatures ($T_1 = 303$ K and $T_2 = 363$ K), for three different total atomic number densities, n_a , falling within the low (Fig. 3 (a)), middle (Fig. 3 (b)) and high-density regions (Fig. 3 (c)) of the experimental measurement range. Each spectrum is integrated over 100 laser shots to increase the signal to noise ratio as well as reduce the influence due to the fluctuation of the drive laser pulse energy (typically $\sim 5\%$). For measuring the HH spectra in the low-density region, the density is set to around $1.6 \times 10^{17} \text{ cm}^{-3}$ (with $p_0=1.5$ bar at $T_1 = 303$ K, $p_0=1.8$ bar at $T_2 = 363$ K). In the middle and high-density regions, the densities are set to around $4.5 \times 10^{17} \text{ cm}^{-3}$ (with $p_0=5.0$ bar at $T_1 = 303$ K, $p_0=6.0$ bar at $T_2 = 363$ K) and to around $2.1 \times 10^{18} \text{ cm}^{-3}$ (with $p_0=24$ bar at $T_1 = 303$ K, $p_0=28$ bar at $T_2 = 363$ K). From Fig. 3, it can be seen that the spectra comprise in total

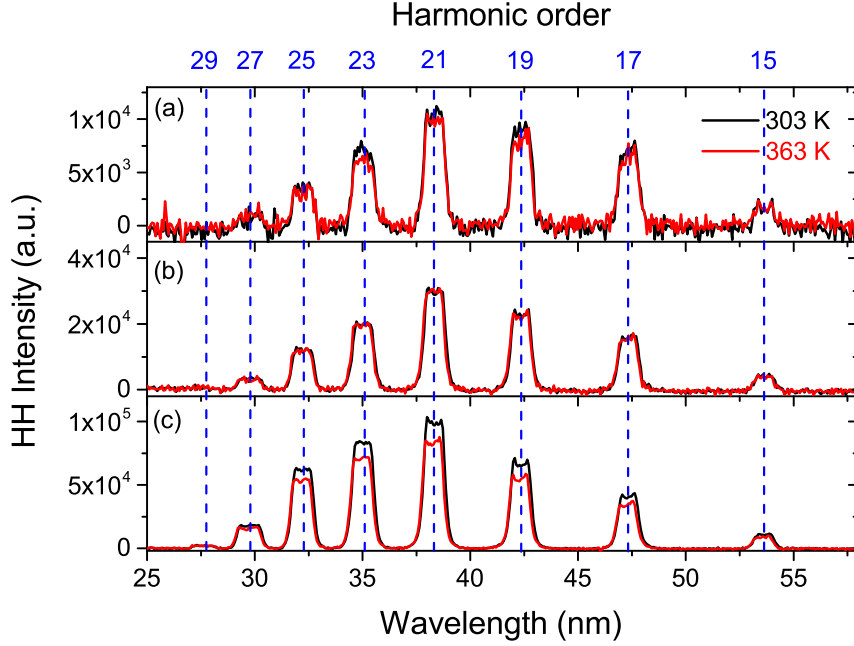


Figure 3: HH spectra measured at 303K and 363 K for the total atomic number densities, $n_a \approx 1.6 \times 10^{17}$ (a), 4.5×10^{17} (b) and $2.1 \times 10^{18} \text{ cm}^{-3}$ (c). The quasi-flat-top shape of the peaks is caused by the limited resolution of the spectrometer, chosen for maximizing the output signal.

eight harmonic orders, ranging from the 15th to the 29th. Note that the 29th harmonic intensity in the low-density region is so weak that it is not observable in the spectrum. Among these harmonic orders, the 21st harmonic consistently exhibits the strongest intensity. Another feature observable in Fig. 3 is that the intensity of the harmonics grows with the increasing total atomic number density, from the low-density region to the high-density region. The HH intensity measured at $T_1 = 303 \text{ K}$ is found to be very similar to that measured at $T_2 = 363 \text{ K}$ in both the low and the middle-density regions, while it is slightly higher in the high-density region. Remarkably, we find that the relative shape of the spectra remains identical, independent of the total atomic number density and the temperature. This suggests that the two-field combinations originating from clusters on one hand and gas monomers on the other hand are emitted coherently, i.e., without any change in relative phase, when the density is increased. On the long wavelength side, the spectra are limited to about 53 nm (15th order). This limit can be traced back to strong reabsorption of the generated XUV radiation in argon [32]. On the short wavelength side, the spectra are limited to about 28 nm (29th order). This wavelength agrees well with the calculated cut-off wavelength according to the three-step model ($\lambda_{\text{cutoff}} = hc/(I_p + 3.17U_p) \approx 28 \text{ nm}$, where U_p is calculated from the experimental laser parameters). Nevertheless, the measured cut-off wavelengths could imply different mechanisms acting in the recombination process during HHG. Specifically, for HHG

in cluster jets, a huge extension of the cut-off wavelength towards shorter wavelengths was previously observed, which has been explained by the so-called atom-to-neighbour collision mechanism [16, 19, 33]. Our observation of the cut-off wavelength does not show such an extension in the measured wavelength range. Instead, the cut-off coincides with the predicted value from the three-step model, as confirmed by experiments of others, suggesting that the coherent emission from clusters is due to the recombination of the tunnel ionized electron with its parent ion within the cluster (atom-to-itself collision mechanism) [17, 18].

Further investigating the high-order harmonic contribution from clusters and gas monomers, we record the harmonic spectra over a broad range of the total atomic number density, n_a , from $n_a = 6 \times 10^{16} \text{ cm}^{-3}$ to $n_a = 2.5 \times 10^{18} \text{ cm}^{-3}$. Since the relative HH intensity distribution in the measured spectra does not change with density (see Fig. 3), it allows us to select, as an example, the 21st harmonic ($\approx 38 \text{ nm}$) in the spectra as representative also for the other harmonic orders. The motivation of choosing the 21st harmonic is that it provides the highest signal in all the spectra and therefore provides the highest signal to noise ratio. In Fig. 4, we plot the average 21st harmonic yield

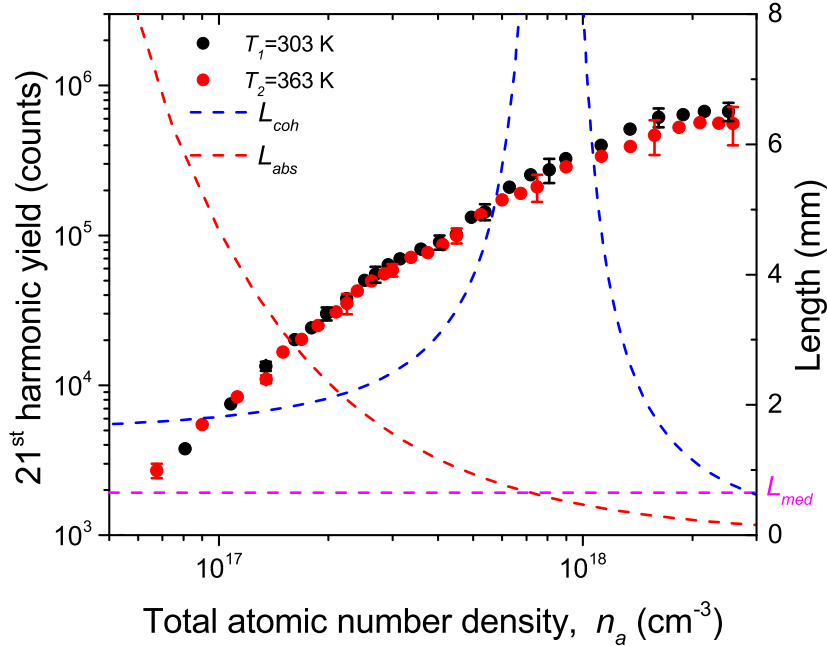


Figure 4: Comparison of the average yield (over 100 shots) at the 21st harmonic as a function of the total atomic number density, n_a , for two different reservoir temperatures, $T_1 = 303 \text{ K}$ (black) and $T_2 = 363 \text{ K}$ (red) respectively. The calculated coherence length (blue dashed curve) and absorption length (red dashed curve) for the 21st harmonic as well as the medium length ($L_{med} = 0.65 \text{ mm}$, pink dashed line) are presented for comparison.

obtained by spectrally integrating the 21st harmonic signal in the spectra, versus the total atomic number density, n_a , for two different temperatures in a double logarithmic scale. Due to weak, single-shot signals of the measured HH spectrum, especially for the measurements at low densities, the error bars shown in Fig. 4 are derived from measurements of the shot-to-shot fluctuations in the relative harmonic beam energy (in total 100 shots), assuming that the relative error in the average spectral intensity is equal to the relative error in the harmonic beam energy. From Fig. 4, it can be seen that the 21st harmonic yield exhibits the same growth for both temperatures, except for some smaller deviation at high densities ($n_a \geq 7 \times 10^{17} \text{ cm}^{-3}$), that remains within the experimental fluctuation of the harmonic yield ($\sim 10\%$, after averaging over 100 pulses), where the HH yield starts to saturate. We also notice that the HH yield summed up over all harmonic orders in the spectra, i.e., from the 15th harmonic to the 27th harmonic, gives a similar growth trend.

Before conclusions can be drawn on the single-particle (clusters or gas mono-mers) contribution to the HH yield, the influence of the absorption as well as the phase mismatch should be minimized. For finding the appropriate experimental density range, we plot the absorption length (L_{abs} , red dashed curve) and the coherence length (L_{coh} , blue dashed curve) in Fig. 4 versus the atomic number density for comparison with the effective experimental interaction length (effective length of the medium, $L_{med} = 0.65 \text{ mm}$, pink dashed line as determined in Ref [26]).

The absorption length, starting with a rather big value, $L_{abs} = 6.5 \text{ mm}$, drops gradually with increasing total number density, n_a . The length becomes smaller than the length of the medium at higher densities ($n_a \geq 7 \times 10^{17} \text{ cm}^{-3}$), which means that here the measured 21st harmonic yield is mainly limited by reabsorption in the jet and, therefore, may mask the behaviour of the cluster size. To ensure that the influence of absorption on HH yield can be neglected at the lower densities below $n_a = 7 \times 10^{17} \text{ cm}^{-3}$, we checked the HH yield for all different harmonic orders, and found no obviously different growth trend below $n_a = 7 \times 10^{17} \text{ cm}^{-3}$ among the different harmonics. Such similarity in the growth trend indicates that here the absorption does not play an important role for the HH yield. As the absorption length is strongly wavelength dependent, the yield should also become strongly dependent on the harmonic orders (with the largest difference between the 15th harmonic and the 27th harmonic) if absorption would play a role.

The coherence length, L_{coh} , is calculated from the wave-vector mismatch consisting of the atomic, the plasma, and the geometric dispersion [34]. It can be noticed that L_{coh} remains at least three to four times longer than L_{med} for a broad range of densities. In the range from $n_a = 5 \times 10^{16} \text{ cm}^{-3}$ to $n_a = 3 \times 10^{17} \text{ cm}^{-3}$, the wave-vector mismatch is mainly dominated by the geometry dispersion originating from the Gouy phase shift, which is independent of n_a . Further increasing n_a , L_{coh} grows rapidly and reaches its maximum value around $n_a = 8 \times 10^{17} \text{ cm}^{-3}$ where the minimum wave-vector mismatch is achieved. Below $n_a = 8 \times 10^{17} \text{ cm}^{-3}$, a maximum variation of 10% in the HH output is theoretically expected when phase mismatch is taken into consideration in the density range around $n_a = 7 \times 10^{16} \text{ cm}^{-3}$. For $n_a > 8 \times 10^{17} \text{ cm}^{-3}$, L_{coh} drops

dramatically due to the dispersion of a large density of ionized electrons and becomes even shorter than L_{med} around $n_a = 2.5 \times 10^{18} \text{ cm}^{-3}$, i.e., here the HH yield is strongly influenced by phase mismatch such that the high-pressure range cannot be analyzed straightforwardly for a cluster-size dependent atomic nonlinearity. For a convincing evaluation without significant influence of absorption and phase mismatch, we limit ourselves to the measured HH yield at densities below $n_a = 7 \times 10^{17} \text{ cm}^{-3}$. Here the measured HH yield is dominated by the single-atom response of single particles.

To derive the relative single-atom response from the clusters and gas monomers, we propose a simple model that includes the liquid mass fraction, g , to interpret the dependence of the HH yield on the total atomic number density, n_a . The liquid mass fraction, g , was misrepresented in previous experiments by simply assuming $g = 1$. Instead, g is essential for evaluating the harmonic contribution from clusters and cannot be generalized as single representing value. The value of g determines the fraction of atoms in the form of differently sized clusters with an average size, $\langle N \rangle$, that may generate harmonics with a different efficiency than the efficiency of the gas monomers, and therefore g affects the HH yield. In other words, if atoms provide a different yield, depending on whether they are part of a cluster or not, the HH output will be different when changing g while maintaining n_a constant. In our model, we follow the basic approach of Durfee et al. and Constant et al. [32, 7]. Here the generated harmonic field from gas monomers or individual atoms which form clusters scales proportionally with the harmonic dipole amplitude and with the atomic number density, when absorption and phase matching terms can be neglected. Consequently, the generated q^{th} harmonic field contributions from gas monomers, $E_{mo}(q)$, and from clusters, $E_{cl}(q)$, can be written as follows:

$$E_{mo}(q) \propto d_{mo}^q \cdot n_{mo}, \quad (1)$$

$$E_{cl}(q) \propto d_{cl}^q(\langle N \rangle) \cdot n_{cl}, \quad (2)$$

where d_{mo}^q and $d_{cl}^q(\langle N \rangle)$ represents the q^{th} harmonic dipole amplitude induced in gas monomers and in the individual atoms inside clusters with an average cluster size, $\langle N \rangle$. n_{mo} and n_{cl} are the atomic number densities for gas monomers and clusters, respectively. By introducing the liquid mass fraction, g , these two terms can be described in terms of the liquid mass fraction, g , and the total atomic number density, n_a , as: $n_{mo} = [1 - g(\langle N \rangle, T)] n_a$, and $n_{cl}(\langle N \rangle) = g(\langle N \rangle, T) n_a$. With these parameters, Eqs.(1) and (2) can be re-written as:

$$E_{mo}(q) \propto d_{mo}^q [1 - g(\langle N \rangle, T)] n_a, \quad (3)$$

$$E_{cl}(q) \propto d_{cl}^q(\langle N \rangle) g(\langle N \rangle, T) n_a. \quad (4)$$

Assuming that the generated harmonic field by gas monomers and clusters add up coherently, the measured HH yield, $\xi(q)$, will scale with the square of the sum of both fields, which can be expressed as

$$\begin{aligned} \xi(q) &\propto [E_{mo}(q) + E_{cl}(q)]^2 \\ &= C [d_{mo}^q (1 - g(\langle N \rangle, T)) + d_{cl}^q(\langle N \rangle) g(\langle N \rangle, T)]^2 \cdot n_a^2, \end{aligned} \quad (5)$$

where C is a wavelength dependent calibration factor, that takes into account the efficiency with which the harmonic radiation emitted from the jet reaches the XUV CCD camera, including the reflectance of the fused silica plate, the transmission of the Al filters and the grating, as well as the responsivity of the camera. To determine the relative single-atom response for gas monomers and clusters using our model, we re-plot from Fig. 4, the HH yield for the 21st harmonic for two different temperatures separately in Fig. 5 (a) and (b) versus the total atomic number density (lower axes) as well as versus the average cluster size (upper axes). The average cluster size, $\langle N \rangle$, that corresponds to the total atomic number density, n_a , is displayed on the top axis of both figures. $\langle N \rangle$ is determined from the stagnation pressures, p_0 and the two specific temperatures, $T_1 = 303$ K and $T_2 = 363$ K, using Hagen's law (for $\langle N \rangle < 1000$) and the newly developed power law (for $\langle N \rangle \geq 1000$) from Ref [26]. The calculated liquid mass fraction, g , for both temperatures is also plotted for comparison. It can be seen that, for both temperatures, the HH yield initially grows rather rapidly, up to $n_a = 3 \times 10^{17} \text{ cm}^{-3}$, where $\langle N \rangle$ is around 1000 atoms per cluster. Specifically, the growth of the HH yield for both temperatures can be fitted, on the double-logarithmic scale of the graph, by the same linear relation (red solid line) with a slope of 2 ± 0.05 and the same interception on the vertical axis of the graphs at -30.1 ± 0.05 . Since the slope has a fitted value of two with a rather small error, we conclude that, simply, the HH yield scales with the square of the total atomic number density, namely, $\xi(\text{HH21}) \propto n_a^2$. According to our model, such a quadratic growth implies that the term $C [d_{\text{cl}}^{\text{HH21}}(\langle N \rangle)g(\langle N \rangle, T) + d_{\text{mo}}^{\text{HH21}}(1 - g(\langle N \rangle, T))]$ in Eq. 5, is independent of n_a , and remains the same for two different chosen temperatures (T_1 and T_2). Since we keep all the experimental settings the same, including the exposure time and gain setting of the camera when recording the spectra at different temperatures, the calibration factor C remains unchanged. Therefore a rather simple relation for the two temperatures can be derived as follows

$$[d_{\text{cl}}^{\text{HH21}}(\langle N \rangle) - d_{\text{mo}}^{\text{HH21}}] g(\langle N \rangle, T_1) = [d_{\text{cl}}^{\text{HH21}}(\langle N \rangle) - d_{\text{mo}}^{\text{HH21}}] g(\langle N \rangle, T_2). \quad (6)$$

In this relation, $d_{\text{cl}}^{\text{HH21}}(\langle N \rangle)$ and $d_{\text{mo}}^{\text{HH21}}$ are intrinsic properties of the particles and therefore are independent on the stagnation pressure and the reservoir temperature. The liquid mass fraction, g , as shown in Fig. 5, however, remains varying with the stagnation pressure and the reservoir temperature and, importantly, has a different dependence on n_a and $\langle N \rangle$ for the two temperatures. This means that for the same $\langle N \rangle$, at different temperatures, e.g., T_1 and T_2 , $g(\langle N \rangle, T_1) \neq g(\langle N \rangle, T_2)$. As a result, Eq. (6) yields that $d_{\text{cl}}^{\text{HH21}}(\langle N \rangle) = d_{\text{mo}}^{\text{HH21}}$. This solution leads to the conclusion that below $n_a = 3 \times 10^{17} \text{ cm}^{-3}$, these clusters with average cluster sizes, $\langle N \rangle$, up to ~ 1000 atoms per cluster can be treated as an ensemble of independent atoms in terms of the HH yield that they generate. In other words, these atoms inside small clusters provide the same single-atom nonlinear response as the gas monomers, resulting in the same harmonic generation efficiency. Note that we do not observe a faster growth trend than the quadratic growth for the 21st harmonic yield with $\langle N \rangle$ up to 700 atoms per

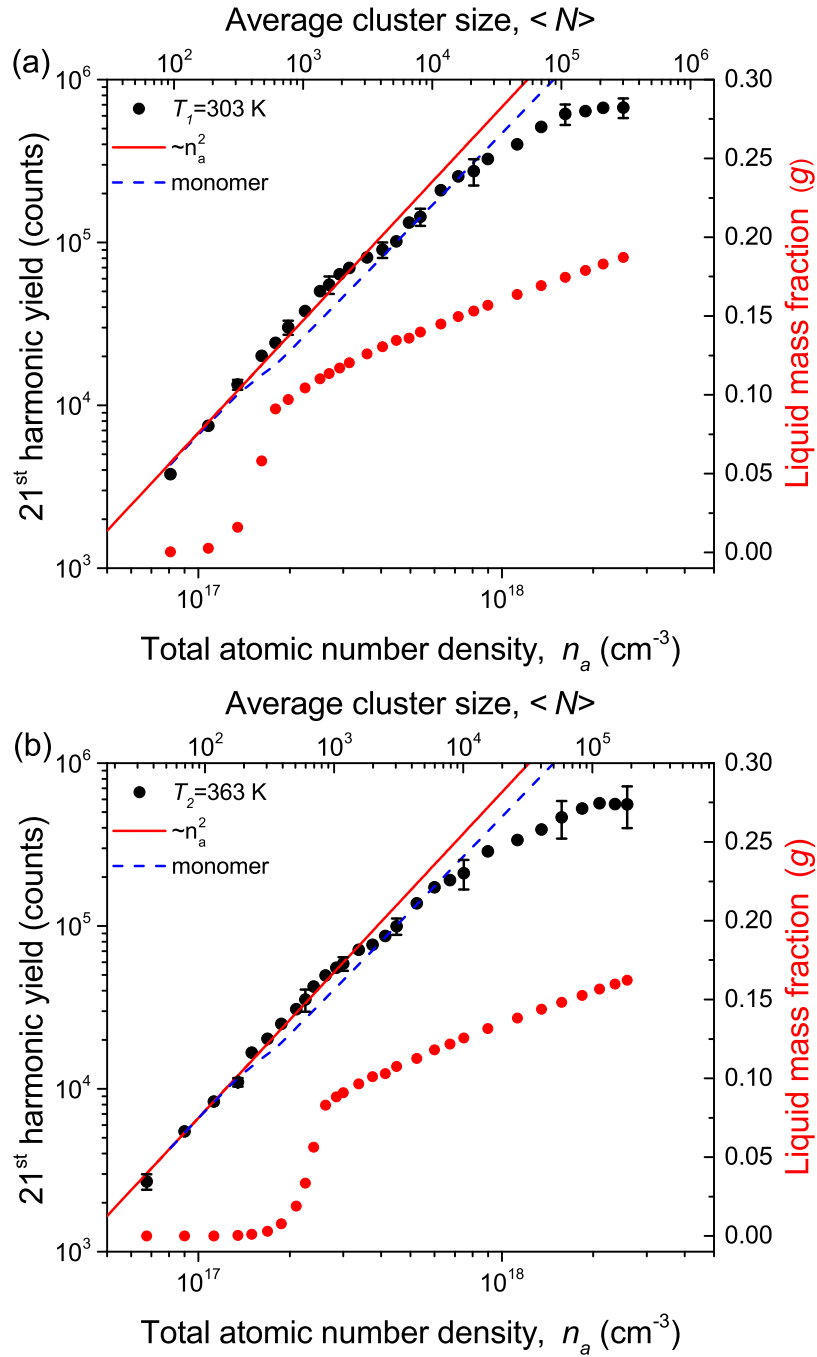


Figure 5: Detailed plot of the 21st harmonic yield versus the total atomic number density, n_a at two different temperatures ($T_1 = 303$ K (a) and $T_2 = 363$ K (b)). The corresponding average cluster size, $\langle N \rangle$, is displayed at the top axes. The liquid mass fraction, g , is plotted in both figures as well. The red solid lines show a $\xi_{\text{HH21}} \propto n_a^2$ relation. For comparison, the blue dashed lines show the 21st harmonic yield generated only from the gas monomers.

cluster. This is in clear contrast to the conclusion drawn by Park et al. [18], who suggest that their observed growth of the yield with n_a results from a larger harmonic dipole amplitude for individual atoms in clusters due to their partial delocalization of the initial wave function.

Above $n_a = 3 \times 10^{17} \text{ cm}^{-3}$ ($\langle N \rangle > 1000$ atoms per cluster), a relatively slower growth trend (less than quadratic) is observed with increasing densities. Using our model with the calculated values of g , we can retrieve the HH yield from only gas monomers for both temperatures, namely, by setting $d_{\text{cl}}^{\text{HH21}}(\langle N \rangle)$ to zero in Eq. 5 (blue dashed lines). This HH yield is plotted in both figures as blue dashed curves. It can be seen that the HH yield, for both temperatures, grows slower than quadratic with increasing density. It deviates from the red solid lines indicating a $\xi_{\text{HH21}} \propto n_a^2$ relation and approaches the blue dashed curves. This observation indicates that the harmonic generation from atoms in larger clusters becomes less efficient. Interestingly, such a slower growth trend is indeed also found by Park et al. [18] when the average cluster size produced in their supersonic argon jet becomes larger than 700 atoms per clusters. This relatively slow growth trend has earlier been explained as resulting from field screening of the laser that prevents further tunnel ionization of atoms inside the core of the larger clusters [35], and from stronger reabsorption of the XUV radiation inside the large clusters resulting in the formation of nanoplasmas [36].

4. Conclusion

We have investigated high-order harmonic generation in a supersonic argon gas jet. To identify the contributions of the generated high-order harmonics from *both* clusters and gas monomers, we measured the harmonic spectra over a broad range of the total atomic number densities (from $3 \times 10^{16} \text{ cm}^{-3}$ to $3 \times 10^{18} \text{ cm}^{-3}$) in the jet at two different reservoir temperatures (303 K and 363 K). For the first time in the evaluation of the harmonic yield in such measurements, the detailed variation of the liquid mass fraction, g , versus pressure and temperature is taken into consideration. We determine this fraction and find, consistently, low values of g below 20%, within our range of experimental parameters. Changing the temperature of the nozzle allows us to study the dependence of the HH yield on different values of g and for the average cluster size, $\langle N \rangle$, while maintaining the value for the total atomic number density, n_a . Based on different values for g at two different temperatures, a simple model is applied to interpret the measured, density-dependent harmonic spectra. We show that the single-atom response in clusters is the same as the response of gas monomers, for clusters having an average size, $\langle N \rangle$, below ~ 1000 atoms per cluster. With increasing $\langle N \rangle$, HHG in clusters becomes less efficient. We also observe no change of the cut-off energy in the measured harmonic spectra, which indicates that the three-step model is still applicable for HHG in clusters, i.e., the tunnel ionized electrons collide with their parent ion. We conclude that using a supersonic gas jet to provide clusters as the nonlinear medium, does not promise a higher harmonic yield via an increased nonlinearity as compared to a gas jet

of monomers. With this finding the use of cluster jets in high-order harmonic generation would rather be that an increased density contrast can be obtained for pursuing a higher yield via quasi-phase matching, such as by placing an array of obstacles.

Acknowledgments

This research was supported by the Dutch Technology Foundation STW, which is part of the Netherlands Organization for Scientific Research (NWO), and partly funded by the Ministry of Economic Affairs (Project No. 10759).

Reference

- [1] Salieres P, L’Huillier A and Lewenstein M 1995 *Phys. Rev. Lett.* **74** 3776
- [2] Uiberacker M, Uphues T, Schultze M, Verhoef A J, Yakovlev V, Kling M F, Rauschenberger J, Kabachnik N M, Schrder H, Lezius M, Kompa K L, Muller H G, Vrakking M J J, Hendel S, Kleineberg U, Heinzmann U, Drescher M and Krausz F 2007 *Nature* **446** 627
- [3] Witte S, Tenner V T, Noom D W E and Eikema K S E 2014 *Light-Sci. Appl.* **3** e163
- [4] He X, Miranda M, Schwenke J, Guilbaud O, Ruchon T, Heyl C, Georgadiou E, Rakowski R, Persson A, Gaarde M B and L’Huillier A 2009 *Phys. Rev. A* **79**
- [5] Corkum P B 1993 *Phys. Rev. Lett.* **71** 1994
- [6] Lewenstein M, Balcou P, Ivanov M Y, L’Huillier A and Corkum P B 1994 *Phys. Rev. A* **49** 2117
- [7] Constant E, Garzella D, Breger P, Mvel E, Dorrer C, Le Blanc C, Salin F and Agostini P 1999 *Phys. Rev. Lett.* **82** 1668
- [8] Hergott J F, Kovacev M, Merdji H, Hubert C, Mairesse Y, Jean E, Breger P, Agostini P, Carr B and Salieres P 2002 *Phys. Rev. A* **66** 021801
- [9] Hadrich S, Klenke A, Rothhardt J, Krebs M, Hoffmann A, Pronin O, Pervak V, Limpert J and Tunermann A 2014 *Nat. Photon.* **8** 779
- [10] Ghimire S, Dichiara A D, Sistrunk E, Agostini P, Dimauro L F and Reis D A 2011 *Nat. Phys.* **7** 138
- [11] Vampa G, Hammond T J, Thire N, Schmidt B E, Legare F, McDonald C R, Brabec T, Klug D D and Corkum P B 2015 *Phys. Rev. Lett.* **115** 193603
- [12] Ndabashimiye G, Ghimire S, Wu M, Browne D A, Schafer K J, Gaarde M B and Reis D A 2016 *Nature* **534** 520
- [13] Wu M X, Ghimire S, Reis D A, Schafer K J and Gaarde M B 2015 *Phys. Rev. A* **91** 043839
- [14] Donnelly T D, Ditmire T, Neuman K, Perry M D and Falcone R W 1996 *Phys. Rev. Lett.* **76** 2472
- [15] Tisch J W G, Ditmire T, Fraser D J, Hay N, Mason M B, Springate E, Marangos J P and Hutchinson M H R 1997 *J. Phys. B* **30** L709
- [16] Vozzi C, Nisoli M, Caumes J P, Sansone G, Stagira S, De Silvestri S, Vecchiocattivi M, Bassi D, Pascolini M, Poletto L, Villoresi P and Tondello G 2005 *Appl. Phys. Lett.* **86** 1
- [17] Ruf H, Handschin C, Cireasa R, Thire N, Ferre A, Petit S, Descamps D, Mevel E, Constant E, Blanchet V, Fabre B and Mairesse Y 2013 *Phys. Rev. Lett.* **110** 083902
- [18] Park H, Wang Z, Xiong H, Schoun S B, Xu J L, Agostini P and DiMauro L F 2014 *Phys. Rev. Lett.* **113** 5
- [19] Aladi M and Foldes I B 2014 *J Phys Conf Ser* **508** 012016
- [20] York A G, Milchberg H M, Palastro J P and Antonsen T M 2008 *Phys. Rev. Lett.* **100** 195001
- [21] Aladi M, Bolla R, Racz P and Foldes I B 2016 *Nucl. Instrum. Meth. B.* **369** 68
- [22] Quere F, Thauray C, Monot P, Dobosz S, Martin P, Geindre J P and Audebert P 2006 *Phys. Rev. Lett.* **96** 125004
- [23] Saalman U 2006 *J. Mod. Opt.* **53** 173

- [24] Dorchie F, Blasco F, Caillaud T, Stevefelt J, Stenz C, Boldarev A S and Gasilov V A 2003 *Phys. Rev. A* **68** 232011
- [25] Smith R A, Ditmire T and Tisch J W G 1998 *Rev. Sci. Instrum.* **69** 3798
- [26] Tao Y, Hagmeijer R, van der Weide E T A, Bastiaens H M J and Boller K J 2016 *J. Appl. Phys.* **119** 164901
- [27] Gao X, Wang X, Shim B, Arefiev A V, Korzekwa R and Downer M C 2012 *Appl. Phys. Lett.* **100** 064101
- [28] Gao X, Arefiev A V, Korzekwa R C, Wang X, Shim B and Downer M C 2013 *J. Appl. Phys.* **114**
- [29] Goh S J, Reinink J, Tao Y, van der Slot P M J, Bastiaens H J M, Herek J L, Biedron S G, Milton S V and Boller K J 2016 *Opt. Express* **24** 1604
- [30] Goh S J, Bastiaens H J M, Vratzov B, Huang Q, Bijkerk F and Boller K J 2015 *Opt. Express* **23** 4421
- [31] Shim B, Hays G, Zgadza j R, Ditmire T and Downer M C 2007 *Phys. Rev. Lett.* **98** 123902
- [32] Durfee Iii C G, Rundquist A R, Backus S, Herne C, Murnane M M and Kapteyn H C 1999 *Phys. Rev. Lett.* **83** 2187
- [33] Zaretsky D F, Korneev P and Becker W 2010 *J. Phys. B* **43** 105402
- [34] Kazamias S, Daboussi S, Guilbaud O, Cassou K, Ros D, Cros B and Maynard G 2011 *Phys. Rev. A* **83** 063405
- [35] Saalman U, Ch S and Rost J M 2006 *J. Phys. B* **39** R39
- [36] Hoffmann K, Murphy B, Kandadai N, Erk B, Helal A, Keto J and Ditmire T 2011 *Phys. Rev. A* **83** 043203